

## Fabrication of super-sharp nanowire atomic force microscope probes using a field emission induced growth technique

A. B. H. Tay and J. T. L. Thong<sup>a)</sup>

*Centre for Integrated Circuit Failure Analysis and Reliability (CICFAR), Faculty of Engineering, National University of Singapore, 4 Engineering Drive 3, Singapore 117576, Singapore*

(Received 22 March 2004; accepted 16 July 2004; published 20 September 2004)

A relatively simple and consistent technique based on field emission induced growth has been developed to grow a single metallic nanowire on an atomic force microscope (AFM) tip. A clamping setup with two micromanipulators ensures that the fabrication of a vertically aligned nanowire probe, which is sharp, robust, and with high aspect ratio, can be achieved on different types of AFM cantilevers with different force constants. The controlled growth technique has been used to produce tungsten nanowire AFM probes with great consistency and high reproducibility. The tungsten nanowires were grown to lengths between 100 nm to 1.5  $\mu\text{m}$  with radius of curvature at the tip end typically between 1–2 nm. Experiments using the fabricated tungsten nanowire AFM probe demonstrate its ability to produce high-resolution AFM images and improved profiling of structures with steep sidewalls due to its very sharp tip and high aspect ratio. The technique can be extended to fabricating other types of metallic nanowire AFM probes or even composite nanowire AFM probes by using different precursor gases. Experiments have been successful in fabricating cobalt nanowire AFM probes which are able to produce good high-resolution AFM images as well. © 2004 American Institute of Physics. [DOI: 10.1063/1.1791321]

### I. INTRODUCTION

Atomic force microscopy<sup>1</sup> (AFM) has taken on greater importance with the growing interest and rapid developments in nanotechnology. Its high-resolution capabilities for surface studies down to atomic levels<sup>2–4</sup> have made it an important tool. Sharp tips with high aspect ratio are thus required for AFM imaging to reduce the distortion of the images associated with the shape of the tip.<sup>5,6</sup> Many different techniques of making very sharp tips with high aspect ratio have been demonstrated by other researchers; these include using focused ion beam etching,<sup>7,8</sup> electron beam induced deposition (EBID)<sup>9</sup>, attaching thin probes, such as a zinc oxide whisker,<sup>10,11</sup> carbon nanotubes (CNT)<sup>12–19</sup> and other nanotubes or nanowires,<sup>20,21</sup> to conventional etched silicon AFM tips. Among which, CNT probes have attracted the most attention due to their high aspect ratio, robustness, high electrical conductivity, chemical inertness, and ability to be functionalized.

Here we report the growth of a single metallic nanowire on existing commercial etched silicon AFM tips by a field emission induced growth technique<sup>22</sup> in the ambient of a suitable precursor gas. Although fabrication of nanowires has been successfully achieved by many different techniques such as vapor-liquid-solid growth,<sup>23–25</sup> solution-solid-liquid growth,<sup>26–28</sup> solvothermal method,<sup>29</sup> laser ablation method,<sup>30–33</sup> template-mediated methods that uses zeolites, membranes or nanotubes,<sup>33–37</sup> and several other methods,<sup>38–41</sup> most methods demonstrated are not suitable

for fabricating a single nanowire directly for use as an AFM probe. The fabrication of a single nanowire on an AFM tip requires accurate positioning so as to ensure only a single nanowire is precisely fabricated at or attached to the tip end of the AFM tip in a vertical manner with great consistency and high reproducibility. Our technique to fabricate a single nanowire on an AFM tip is a relatively simple technique with great control over the characteristics of the single nanowire and with high reproducibility.

It was previously reported that metallic needle-like structures were formed on electron-emitting regions of a cathode surface when operated in a vacuum containing metal carbonyl vapors.<sup>42–44</sup> The metallic whiskers formed grew in an uncontrolled manner and resembled tree-like structures with very sharp ends. The field emission induced growth technique adopts a similar approach to fabricate a single metallic nanowire with control over the position and length of the nanowire grown. An early technique previously reported<sup>21</sup> uses a two-step field emission induced growth process to fabricate tungsten nanotips which are relatively long and of a thicker shank diameter, so as to provide imaging stability. However, the method does not always yield vertically aligned probes and could also result in random forking of the grown nanowire. The current method uses a proximal probe as the anode for field emission and operates in a lower field emission current regime to eliminate the forking phenomenon that could arise with the earlier method. The resulting finer axially aligned vertical nanometer probe is joined to the apex of a conventional etched silicon AFM tip.

<sup>a)</sup> Author to whom correspondence should be addressed; electronic mail: elettl@nus.edu.sg

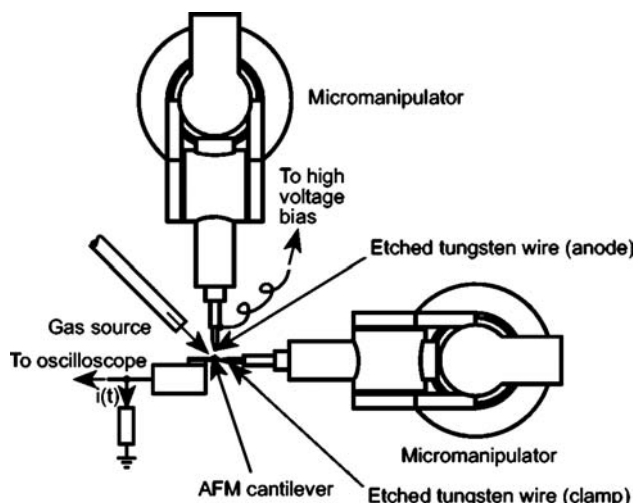


FIG. 1. Schematic of the top view of the setup in the ESEM for the growth of a single nanowire on a silicon etched AFM tip.

II. EXPERIMENT

The controlled growth of a single metallic nanowire on an AFM tip (BS-Tap300A1, BudgetSensors) is carried out in a high vacuum chamber of an environmental scanning electron microscope (ESEM) (XL30 ESEM FEG, Philips). The ESEM is operated in conventional high-vacuum mode, but with the pressure limiting apertures in place to limit the flow of precursor gas into the column. Two three-axis micromanipulators (MM3-EM, Kleindiek Nanotechnik), are each fitted with an electrochemically etched tungsten sharp tip (Fig. 1). The small step size of  $\sim 5$  nm of the micromanipulator allows the etched tungsten tips to be positioned accurately at their desired positions. One of the tungsten sharp tips is used as an anode for the field emission induced growth process while the other is used to hold down the AFM cantilever (Fig. 2). This is to prevent the AFM cantilever from bending due to the attractive force present when a positive voltage bias is applied between the anode and the cathode (the AFM tip where the tungsten nanowire is to be grown) during the

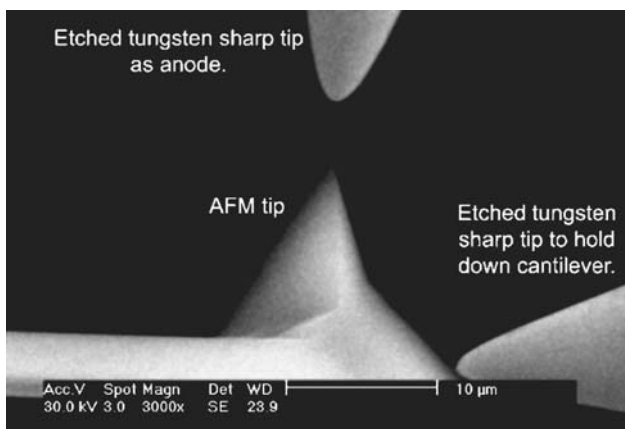


FIG. 2. SEM image showing precise positioning of the etched tungsten sharp tips attached to the ends of each micromanipulator for the field emission induced growth. One of the etched tungsten sharp tips is used to hold down the cantilever in a clamping setup to prevent the cantilever from bending toward the anode when a positive voltage bias is applied.

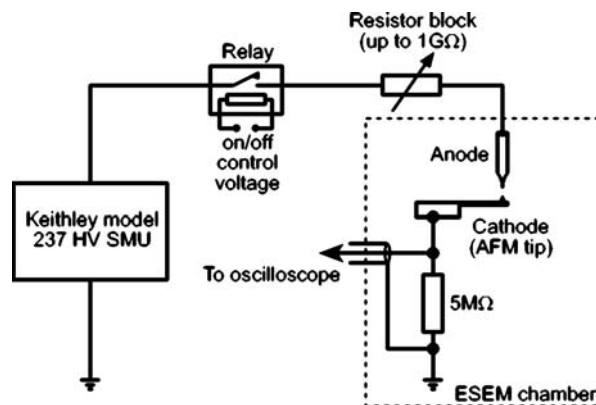


FIG. 3. Electrical circuit used for the field emission induced growth process. The SMU is controlled by a computer.

field emission induced growth process. The ESEM provides high-resolution viewing capabilities to assist in the precise positioning of the anode, which has to be aligned vertically with the AFM tip (cathode) in three dimensions, as well as *in situ* viewing of the tungsten nanowire grown. A gas nozzle, placed at a  $45^\circ$  incline approximately 1 cm away from the AFM tip and directed toward the AFM tip, is used to provide the precursor gas for the field emission induced growth technique. The local gas pressure at the anode and AFM tip region is of the same order as the gas pressure at the nozzle of the gas pipe under molecular flow. By assuming that the gas throughput through the gas nozzle to be equal to the throughput through the diffusion pump of the ESEM, the gas pressure at the nozzle of the gas pipe can be estimated from the chamber pressure and the pumping speed. Hence, a gas pressure of  $3 \times 10^{-5}$  mbar can be converted to a local gas pressure of approximately  $1 \times 10^{-2}$  mbar at the nozzle. Figure 3 shows the electrical circuit for the field emission induced growth process. A source measurement unit (SMU, model 237 Keithley), which is controlled by a computer using in-house software, is used to provide the high voltage supply to the anode for the field emission. The software program allows precise control of the constant field emission current and the growth duration, and also records the voltage readings during the growth process. An oscilloscope (Infinium 54845A, HP) is used to record the field emission current through the AFM tip to monitor the instantaneous field emission current.

The precursor gas used for the growth of a single tungsten nanowire on an AFM tip is tungsten hexacarbonyl,  $W(CO)_6$ . The tungsten carbonyl source is kept in a small aluminum container, which is temperature-controlled at  $35^\circ C$ , and is fed into the ESEM chamber through a variable leak valve. The sample, an etched silicon AFM tip, is first loaded into the ESEM chamber together with two electrochemically etched tungsten sharp tips, one attached to each micromanipulator. The chamber is then pumped down to a base pressure of  $5 \times 10^{-6}$  mbar. Once the required pressure is attained, the electron beam is turned on and the sharp tip end of the anode is aligned with the AFM tip end in three-dimensional space with a small gap of a few micrometers in between. The other etched tungsten sharp tip is positioned to

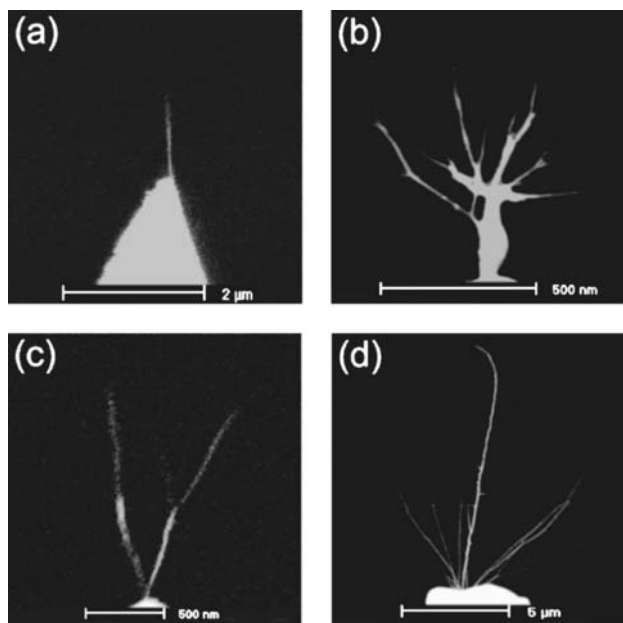


FIG. 4. (a) SEM image of a single vertically aligned tungsten nanowire grown on an AFM tip using a field emission current of 200 nA grown to about 1  $\mu\text{m}$  in length. (b) SEM image of a tree-like structure formed on an AFM tip due to high field emission current applied. (c) SEM image of multiple nanowires growing from the same field emission point on an AFM tip when the field emission current is increased beyond the limit for single nanowire growth. (d) SEM image of a single nanowire dominating the growth after some time despite multiple nanowires grown from the AFM tip initially at high field emission current.

hold down the AFM cantilever so as to prevent it from bending toward the anode due to the attractive electrostatic force that will appear when a voltage bias is applied on the anode. The precursor gas is then administered into the chamber through the variable leak valve. The gas pressure in the chamber is increased to  $3.5 \times 10^{-5}$  mbar and kept constant thereafter throughout the field emission induced growth process. Once the gas pressure has stabilized, the high voltage supply is turned on. The positive bias at the anode will initiate field emission from the tip end of the AFM tip. With the precursor molecules being dissociated by the electrons and attracted to the cathode, a nanowire is formed at the point of field emission. Subsequent field emission from the nanowire wire itself, preferential due to its geometrical enhancement, results in the growth of a single nanowire at the sharp AFM tip end. The length of the single nanowire grown depends on the duration of the field emission process. Once the required duration of growth is achieved, the high voltage supply is turned off and this terminates the growth process. The precursor gas is then shut off and the chamber can then be vented to retrieve the nanowire AFM probe for use in AFM imaging.

### III. RESULTS AND DISCUSSION

Studies on the growth of tungsten nanowires using the field emission induced growth technique found that for the growth of a single tungsten nanowire [Fig. 4(a)] the field emission current has to be less than 200 nA. Higher field emission growth currents result in either a tree-like structure

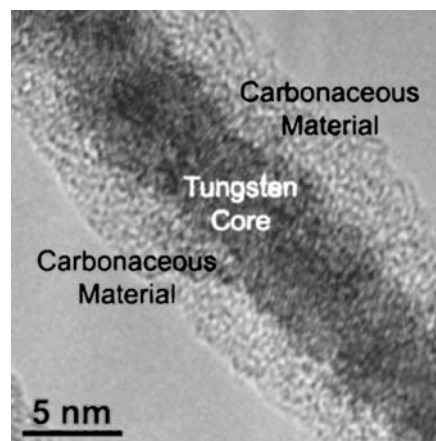


FIG. 5. TEM image of a tungsten nanowire grown on a TEM grid under similar conditions for field emission induced growth of the tungsten nanowire on a silicon etched AFM tip.

[Fig. 4(b)] or multiple nanowires growing from the same field emission point [Fig. 4(c)]. With a higher field emission current, multiple tips can field emit at the same time with the total field emission current shared among the field emitting tips. As the field emission current is never equally distributed, the growth rate of nanowires on the various field emitting tips will be different with tips having a higher field emission current growing at a faster rate. This results in the tips with the faster growing nanowires experiencing a greater field as they approach the anode more rapidly, thereby reducing the cathode to anode spacing, compared to tips with slower growing nanowires. This in turn increases the proportion of the total field emission current emitted by the longer nanowires and reduces the proportion of the total field emission current emitted by the shorter nanowires. When the field emission induced growth process is carried out sufficiently long, the shorter nanowires will cease to grow at some point in time and eventually, only a single long nanowire will take over, emitting most of the total current [Fig. 4(d)]. For field emission growth currents lower than 200 nA, a single tungsten nanowire is formed. Transmission electron microscopy (TEM) studies of the tungsten nanowires grown on a TEM grid with the field-emission induced growth method under similar conditions found that the tungsten nanowire is around 5–10 nm in diameter, comprising a tungsten core of 3–6 nm coated with a layer of low  $Z$  carbonaceous material (Fig. 5). The radius of curvature of the tip of the nanowire is typically less than 1–2 nm, but this could not be ascertained due to the rapid contamination of the tip under electron irradiation.

#### A. Blunting of AFM tip

At the start of the field emission induced growth process where a high positive voltage bias is applied to the anode, a large current spike (observed on the oscilloscope as a voltage spike) occurred at the onset of field emission. A vacuum arc is believed to have occurred. Observation of the AFM tip in the ESEM right after the spike showed that the AFM tip is blunted. The current spike experienced by the silicon AFM tip results in a reduction of approximately 1  $\mu\text{m}$  in the height

of the AFM tip and a rounded region of approximately  $1\ \mu\text{m}$  in diameter. Hence, the blunted tip has a larger radius of curvature as compared with the original tip and the local electric field at the tip will decrease given the same anode voltage. Consequently, field emission is not sustained as the blunted tip is no longer as effective as the original sharp tip as a field emitter and is no longer able to field emit at the same anode voltage. The mechanism behind the blunting of the AFM tip at the onset of the field emission is believed to be due to the occurrence of explosive electron emission<sup>45–48</sup> that led to a vacuum arc. Rapid heating of the sharp AFM tip, with a radius of curvature about  $10\ \text{nm}$ , by the field emission current with densities that can reach  $10^8\ \text{A cm}^{-2}$  or more results in explosive electron emission with an avalanche of electrons being emitted. The thermal instability results in transition from field emission to explosive emission and vacuum arc. In addition, studies on silicon nanowires<sup>49</sup> found that the thermal conductivity observed at such small dimensions is much lower than the bulk value (approximately  $150\ \text{Wm}^{-1}\ \text{K}^{-1}$ ) and is most likely explained by the increased phonon boundary scattering. The lower thermal conductivity means that the heat generated by the field emission current will be conducted away from the hot spot slower and thus contributes to the formation of explosive electron emission. The loss of the material at the sharp tip end after a current spike reinforces the analysis whereby an explosive electron emission occurred during the onset of field emission, resulting in a vacuum arc whereby intense heating of the tip end due to the high current densities causes the material to melt and evaporate.

Several methods were studied to overcome the blunting of the AFM tip which prevents continuous field emission that is needed for the growth of the nanowire. Different metals (nickel, gold, tantalum, and platinum) were used separately to form a very thin coat (via thermal evaporation, e-beam evaporation, or sputtering) over the AFM tip with a view that the metals, having a better electrical and thermal conductivity and higher melting point, will be able to achieve a sustained field emission without the AFM tip blunting. However, the metal coatings that have been tried were unable to provide a solution to the blunting of the AFM tip. At the onset of field emission, the current spike causes the metal coatings to be damaged along with the underlying silicon tip (Fig. 6). Higher thermal conductivity (gold) and electrical conductivity (all metals) and higher melting point (tantalum) were unable to provide a solution to overcome the damage caused by the current spike at the onset of field emission. A commercially available tungsten carbide ( $\text{W}_2\text{C}$ ) coated tip from Mikromasch (Tallinn, Estonia) was also tested under the same conditions as the  $\text{W}_2\text{C}$  coated AFM tip is much harder, in addition to having good thermal and electrical properties. The  $\text{W}_2\text{C}$  coated AFM tip end is also blunted during the initial current spike but to a much lesser extent than the standard etched silicon AFM tip and hence remains sufficiently sharp to maintain the field emission at the same applied voltage bias. Despite being able to provide a sharper tip end for the growth of a single tungsten nanowire, the commercial tungsten carbide coated tip is too costly and inappropriate for it to be used widely. A more cost-effective

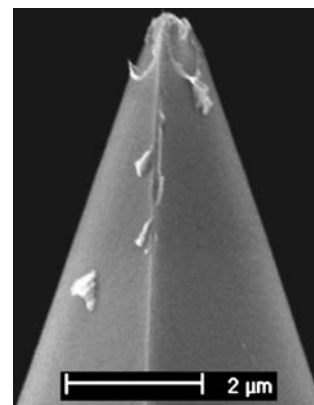


FIG. 6. SEM image of a metal-coated (platinum) AFM tip after experiencing a current spike at the onset of field emission. The metal coating was damaged together with the underlying AFM tip.

solution was found by using the blunted AFM tip to grow a single tungsten nanowire at the tip.

### B. Single tungsten nanowire AFM probe

The process of growing a single tungsten nanowire on the blunted AFM tip continues after the AFM tip has been blunted. As a result of blunting, the gap between the AFM tip and the anode is also increased. Hence, the AFM tip has to be realigned to bring it closer to the anode with approximately  $1\ \mu\text{m}$  apart, while ensuring that the AFM tip and the anode remains vertically aligned. Experiments conducted found that the turn-on voltage required is between  $660$  to  $750\ \text{V}$ , which is higher than that of a sharp AFM tip. The current spike observed at the onset of field emission is followed by a sustained field emission at the controlled constant current (Fig. 7). This sustained field emission results in the initiation of the tungsten nanowire at the field emitting point. Once a tungsten nanowire is formed, electron emission occurs through the formed tip, and the tungsten nanowire grows along the axis. Hence, growth of the tungsten nanowire on the blunted AFM tip is feasible and more cost effective as the blunted AFM tip is not severely deformed to the extent that it is no longer useful for AFM.

Accurate axial alignment of the anode and the AFM tip in three dimensions is important; otherwise, the growth of

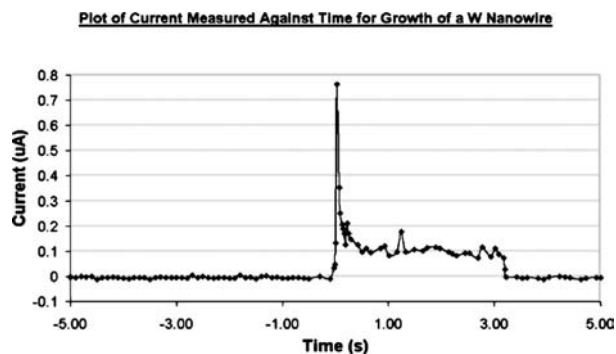


FIG. 7. Oscilloscope measurement showing the current spike experienced followed by sustained field emission at constant current, resulting in the growth of a single tungsten nanowire on a blunted AFM tip for approximately  $3\ \text{s}$ .

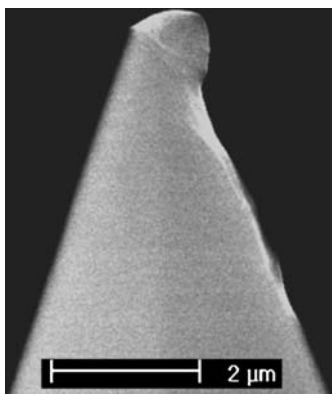


FIG. 8. SEM image of a blunted AFM tip which is slanted as a result of deliberate misalignment between the anode and the AFM tip. This shows that the onset of field emission is the cause of the blunting of the AFM tip as the position of the anode affects the direction in which the blunted tip orientates.

the tungsten nanowire on the AFM tip will not be vertical. Experiments conducted by deliberately placing the anode a distance away from the AFM tip and misaligned axially showed that when a AFM tip is blunted as a result of the initial current spike, it is slanted in the direction toward the anode and the rounded end actually protrudes from the original conical shape of the AFM tip (Fig. 8). This suggests that during the course of the AFM tip melting and evaporating when the current spike is experienced, the high field present plays a part in reshaping the AFM tip such that some of the molten material that cooled down subsequently formed a slanted rounded tip that protrudes out from the original shape of the AFM tip. Growth of the tungsten nanowire on the AFM tip without accurate axial alignment of the anode and the AFM tip results in a slanted nanowire grown. The stringent demand on accurate axial alignment between the anode and the AFM tip is particularly important due to the close proximity between the anode and the AFM tip. Any slight misalignment will result in the grown nanowire having a significant tilt from the vertical axis which is undesirable for it to be used as an AFM probe.

A possible solution is to increase the distance between the anode and the AFM tip. However, this is not desirable as a very high voltage bias is required to field emit the blunted tip at a greater distant apart. Experiments conducted found that the damage due to vacuum arc at the onset of field emission at the higher voltage bias with a bigger gap results in more severe damage. Hence, to avoid using a higher voltage bias, the anode and the AFM tip are first realigned with a small gap to initiate field emission. When field emission occurs and a short tungsten nanowire formed (which can be observed by a large drop in the supplied voltage of the SMU operating in constant current mode) the high voltage supply is quickly turned off. This allows the tungsten nanowire to form on the AFM tip for only approximately one second. The anode is then retracted to a much greater distance, typically up to about  $10\ \mu\text{m}$ , while keeping it axially aligned with the AFM tip. As the tungsten nanowire formed has a greater field enhancement factor than the original silicon AFM tip due to its extremely sharp field emitting point, it is able to field emit

at a lower voltage. Thus the anode can be placed at a greater distance away without having to apply a very high voltage bias for field emission to occur. The voltage supply is then turned on again to continue the growth process for the desired time, yielding vertically aligned single tungsten nanowire of the required length. Due to greater separation, the effect of any slight misalignment is greatly reduced and the tungsten nanowire grown on the AFM tip is generally vertical. A limitation is that such an approach is unable to achieve very short (200 nm or less) tungsten nanowire growth accurately since the growth duration for such short nanowire growth is only  $\sim 3$  s or less. Hence, for the growth of very short nanowires, the axial alignment of the anode and the blunted AFM tip is essential.

It has been discussed earlier that for the growth of a single nanowire, the field emission current is controlled at 200 nA and below. Low field emission currents result in very thin single nanowires, but they cannot be grown long as they are then unable to remain sufficiently rigid. A thin nanowire will not be able to support its own weight and will collapse after the applied voltage bias is removed. Hence, for the growth of longer single nanowires, higher field emission currents (but still less than 200 nA) are used so as to provide the single nanowire with a stronger base to support its own weight. This is important since the single nanowire is used as an AFM probe. Vibrations of the single nanowire will thus compromise the resolution capabilities of the very sharp tip end of the nanowire. Studies carried out found that at a field emission current of 100 nA, a single tungsten nanowire of up to 500 nm in length can be grown and yet remain sufficiently rigid for use in AFM studies. For relatively longer single tungsten nanowires up to approximately  $1.5\ \mu\text{m}$ , a field emission growth current of 200 nA is appropriate.

### C. AFM imaging using tungsten nanowire probe

The tungsten nanowire AFM probe was used in tapping mode AFM imaging to demonstrate its high-resolution capabilities. A sputtered thin gold film on silicon substrate and an evaporated thin platinum film on silicon substrate were used as test samples. A JEOL JSPM-5200 Scanning Probe Microscope is used for the AFM studies. The same type of AFM tips used for fabricating the nanowire probe was used as comparison so as to avoid any improved performance attributed to different cantilever characteristics. High resolution scans of the thin gold film sample using the tungsten nanowire AFM probe [Fig. 9(a)] show an improved topography image with distinct gold grains when compared to the same high resolution scans of the thin gold film, operated under the same conditions and scan speed, using the standard commercial tapping mode AFM tip [Fig. 9(b)].

High resolution scans of the thin platinum film sample using a short tungsten nanowire AFM probe (approximately 400 nm) and a relatively longer tungsten nanowire AFM probe (approximately  $1.2\ \mu\text{m}$ ) show that the image acquired using the longer tungsten nanowire AFM probe [Fig. 10(a)] was not as sharp as the images acquired using the short tungsten nanowire AFM probe [Fig. 10(b)]. This can be attributed to instabilities in the longer tungsten nanowire during tapping mode imaging, either due to the tungsten nanowire vi-

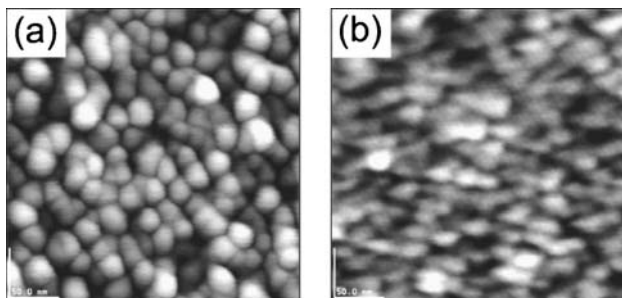


FIG. 9. Tapping mode AFM topography images of a sputtered thin gold film on silicon substrate using (a) a tungsten nanowire AFM probe (displayed height range =3.8 nm) and (b) a standard etched silicon tapping mode AFM tip (displayed height range =3.8 nm). Scan area is 300 nm×300 nm.

brating sideways or due to buckling of the tungsten nanowire or a combination of both. This results in loss of resolution when high-resolution images are acquired. Thus, for very high-resolution images, short tungsten nanowire AFM probes have to be used.

In addition to its high-resolution capabilities, the tungsten nanowire AFM probe, having a high aspect ratio due to the very thin tungsten nanowire, is able to perform well in imaging profiles with trench-like structures or deep holes. The pyramid shape of the standard etched silicon AFM tip limits its capability in profiling structures with deep trenches or holes. Scans of the test sample, a 220 nm thick polymethyl methacrylate (PMMA) resist layer patterned by electron beam lithography to form trench-like structures of 200 nm width and intertrench spacing of 220 nm, using a standard etched silicon tapping mode AFM tip [Fig. 11(a)] and a tungsten nanowire AFM probe [Fig. 11(b)] show that the tungsten nanowire AFM probe is able to profile the trench-like structures much better than the standard AFM tip. Measurements taken from the images show that the width of the trench and the width of the resist at the base of the trench are 148 and 288 nm, respectively, for the standard etched silicon AFM tip, and 188 and 201 nm, respectively, for the tungsten nanowire AFM probe. It can be seen that the standard AFM tip is unable to follow the steep walls of the trench-like structure and the sloping sides produced are attributed to the pyramid shape of the AFM tip. On the other hand, the AFM image obtained using the tungsten nanowire AFM probe shows vertical sidewalls for the trench-like

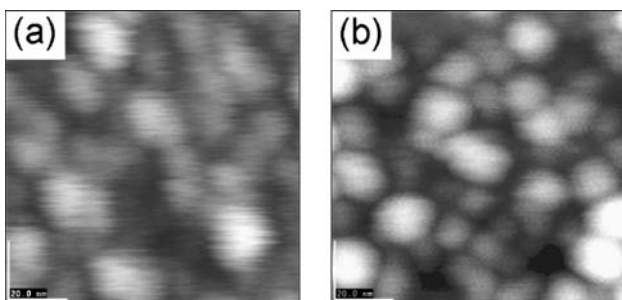


FIG. 10. Tapping mode AFM topography images of an evaporated thin platinum film sample on silicon substrate using (a) a relatively long tungsten nanowire AFM probe, and (b) a short tungsten nanowire AFM probe. Displayed height range =4 nm. Scan area is 100 nm×100 nm.

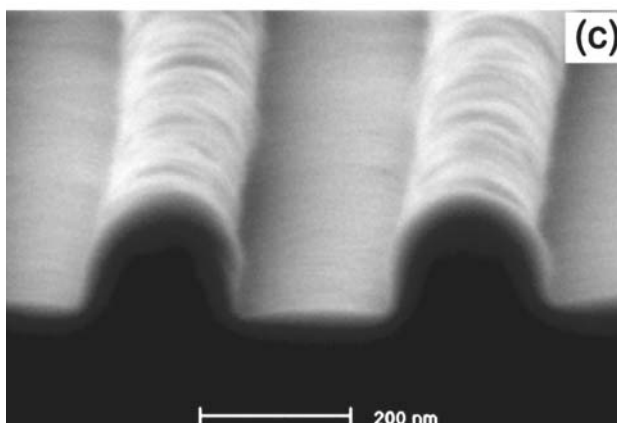
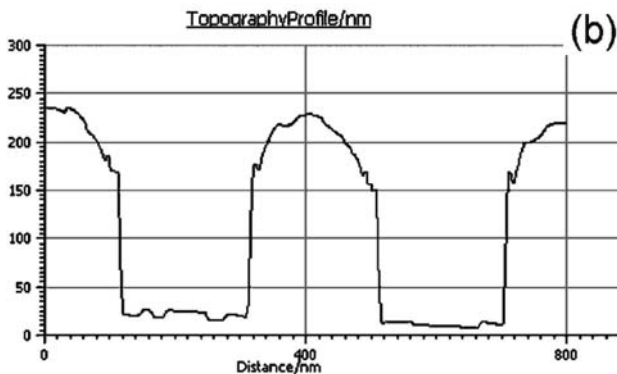
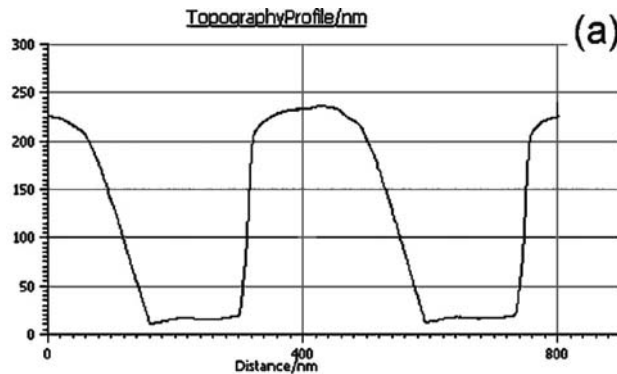


FIG. 11. Cross-sectional profile of the patterned PMMA resist of a trench-like structure obtained from tapping mode AFM scans using (a) a standard etched silicon tapping mode AFM tip and (b) a tungsten nanowire AFM probe. Both scans are carried out at the same scan size and speed. (c) SEM image of the patterned PMMA resist of a trench-like structure.

structure with little asymmetry. The accuracy of the AFM topography obtained is confirmed by viewing the test sample in a scanning electron microscope (SEM) [Fig. 11(c)].

The tungsten nanowire was also grown on AFM tips with a softer cantilever (force constant of 0.2 N/m) to be used for contact mode AFM imaging. Scans of a thin gold film show that the tungsten nanowire AFM probe [Fig. 12(a)] is able to produce clear high resolution images which are comparable to images acquired by the standard contact mode AFM tip [Fig. 12(b)]. The individual gold grains, which can be as small as a few tens of nanometers, are distinctively separated from one another in the image obtained by the tungsten nanowire AFM probe in contact mode AFM. As the standard contact mode AFM tips are able to achieve atomic resolution imaging of flat samples, this simple experiment

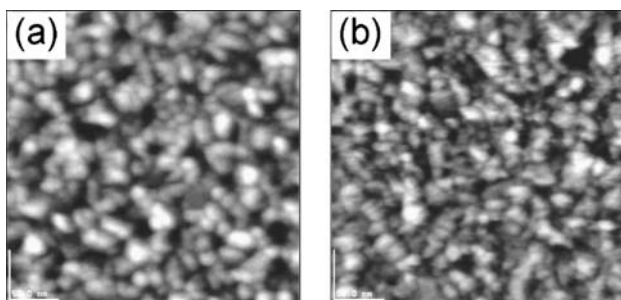


FIG. 12. Contact mode AFM topography images of an evaporated thin gold film on silicon substrate using (a) a tungsten nanowire AFM probe and (b) a standard etched silicon contact mode AFM tip. Scan area is  $300\text{ nm} \times 300\text{ nm}$

does not demonstrate any tangible advantage of the nanowire tip in imaging. However, it can be seen from here that the tungsten nanowire AFM probe can be used in contact mode AFM effectively for high resolution imaging and this may provide possibilities for other applications such as conductive AFM measurements.

Observations in the SEM after tapping mode and contact mode AFM imaging verified that the tungsten nanowire is still present on the AFM tip. In fact, as the tungsten nanowire is grown on blunted AFM tips, a sudden loss in resolution of the AFM image would be observed during AFM imaging in the event that the tungsten nanowire breaks off from the AFM tip.

#### D. Single cobalt nanowire probe

Growth of cobalt nanowire AFM probes were also successfully carried out using the same setup and procedures with cobalt tricarbonyl nitrosyl,  $\text{Co}(\text{CO})_3\text{NO}$ , as the precursor (Fig. 13). The shape of the cobalt nanowire formed is usually thinner at the base, and then it broadens at the center before tapering to a sharp tip at the end due to thermal decomposition of  $\text{Co}(\text{CO})_3\text{NO}$  attributed to Joule heating. In addition, the growth of the cobalt nanowire has a lower ten-

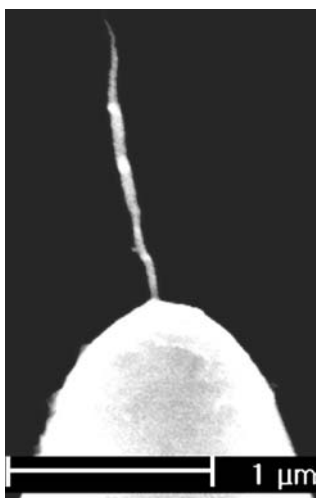


FIG. 13. SEM image of a cobalt nanowire AFM probe. The cobalt nanowire is grown to approximately  $1.2\text{ }\mu\text{m}$  in length at a field emission current of  $300\text{ nA}$ .

dency to form branches or produce multiple nanowires as compared to the growth of tungsten nanowires. Studies found that at up to a field emission current of  $400\text{ nA}$ , a single cobalt nanowire is grown. As the base of the cobalt nanowire grown is relatively thin as compared to its body when a relatively long nanowire is grown, thickening of the base using a relatively coarse and uncontrolled electron-beam induced deposition (EBID) technique is carried out so as to increase the rigidity of the cobalt nanowire at the point of attachment. The cobalt precursor gas is continuously administered into the ESEM chamber during EBID. As the cobalt nanowire may collapse due to the bombardment of the electron beam from the scanning electron microscope while EBID is carried out at the base of the cobalt nanowire, a small positive bias ( $50\text{ V}$ ) is applied on the anode to create an electric field between the cobalt nanowire and the anode so as to keep the cobalt nanowire upright with the attractive force generated by the electric field.

The cobalt nanowire AFM probe was used in tapping mode AFM imaging and is able to produce consistent high-resolution images under continuous scanning for one hour. Attempts to magnetize the cobalt nanowire probe and use it for magnetic force microscopy (MFM) have not been very successful, though viable, as the phase signal contrast was poor. This is believed to be due to the soft magnetic property of pure cobalt. Further studies are currently in progress to improve the MFM contrast.

In conclusion, we have successfully developed a field emission induced growth technique to fabricate a single nanowire AFM probe for AFM studies. The single nanowire AFM probe is able to achieve high-resolution AFM imaging and perform better at profiling deep vertical trenches or holes due to its smaller radius of curvature at the tip end and its higher aspect ratio. The potential of this relatively simple technique in fabricating different metallic nanowire probes by using different precursor gases means that different types of nanowire probes, including composite nanowire probe with two or more different metals, can be fabricated for different purposes. It is also believed that the technique will have other possible applications in other areas of nanotechnology given its relatively simple and well-controlled procedures in fabricating nanowires.

#### ACKNOWLEDGMENTS

This project was funded by a grant from A\*STAR. We would like to thank S. H. Khong for help with the TEM imaging of the nanowire.

<sup>1</sup>G. Binnig and C. F. Quate, *Phys. Rev. Lett.* **56**(9), 930 (1986).

<sup>2</sup>F. J. Giessibl and G. Binnig, *Ultramicroscopy* **42-44**, 281 (1992).

<sup>3</sup>F. J. Giessibl, *Science* **267**, 68 (1995).

<sup>4</sup>Th. Schimmel, Th. Koch, J. Küppers, and M. Lux-Steiner, *Appl. Phys. A: Mater. Sci. Process.* **68**, 399 (1999).

<sup>5</sup>F. F. Abraham and I. P. Batra, *Phys. Rev. Lett.* **60**(13), 1314 (1988).

<sup>6</sup>N. Sasaki and M. Tsukada, *Phys. Rev. B* **52**(11), 8471 (1995).

<sup>7</sup>M. J. Vasile, D. Grigg, J. E. Griffith, E. Fitzgerald, and P. E. Russell, *J. Vac. Sci. Technol. B* **9**(6), 3569 (1991).

<sup>8</sup>J. E. Griffith, H. M. Marchman, G. L. Miller, and L. C. Hopkins, *J. Vac. Sci. Technol. B* **13**(3), 1100 (1995).

<sup>9</sup>D. J. Keller and C.-C. Chou, *Surf. Sci.* **268**, 333 (1992).

<sup>10</sup>H. Kado, K. Yokoyama, and T. Tohda, *Rev. Sci. Instrum.* **63**(6), 3330

- (1992).
- <sup>11</sup>H. Kado, S. Yamamoto, K. Yokoyama, T. Todha, and Y. Umetani, *J. Appl. Phys.* **74**(7), 4354 (1993).
- <sup>12</sup>J. H. Hafner, C.-L. Cheung, T. H. Oosterkamp, and C. M. Lieber, *J. Phys. Chem. B* **105**(4), 743 (2001).
- <sup>13</sup>H. Dai, J. H. Hafner, A. G. Rinzler, D. T. Colbert, and R. E. Smalley, *Nature (London)* **384**, 147 (1996).
- <sup>14</sup>C. V. Nguyen, K. J. Chao, R. M. D. Stevens, L. Delzeit, A. Cassell, J. Han, and M. Meyyappan, *Nanotechnology* **12**, 363 (2001).
- <sup>15</sup>S. S. Wong, J. D. Harper, P. T. Lansbury, Jr., and C. M. Lieber, *J. Am. Chem. Soc.* **120**, 603 (1998).
- <sup>16</sup>R. Stevens, C. Nguyen, A. Cassell, L. Delzeit, M. Meyyappan, and J. Han, *Appl. Phys. Lett.* **77**(21), 3453 (2000).
- <sup>17</sup>E. S. Snow, P. M. Campbell, and J. P. Novak, *Appl. Phys. Lett.* **80**(11), 2002 (2002).
- <sup>18</sup>C. V. Nguyen, R. M. D. Stevens, J. Barber, J. Han, M. I. Sanchez, C. Larson, and W. D. Hinsberg, *Appl. Phys. Lett.* **81**(5), 901 (2002).
- <sup>19</sup>T. Larsen, K. Moloni, F. Flack, M. A. Eriksson, M. G. Lagally, and C. T. Black, *Appl. Phys. Lett.* **80**(11), 1996 (2002).
- <sup>20</sup>A. Rothschild, S. R. Cohen, and R. Tenne, *Appl. Phys. Lett.* **75**(25), 4025 (1999).
- <sup>21</sup>C. H. Oon, J. T. L. Thong, Y. Lei, and W. K. Chim, *Appl. Phys. Lett.* **81**(16), 3037 (2002).
- <sup>22</sup>J. T. L. Thong, C. H. Oon, M. Yeadon, and W. D. Zhang, *Appl. Phys. Lett.* **81**(25), 4823 (2002).
- <sup>23</sup>R. S. Wagner and W. C. Ellis, *Appl. Phys. Lett.* **4**(5), 89 (1964).
- <sup>24</sup>M. K. Sunkara, S. Sharma, R. Miranda, G. Lian, and E. C. Dickey, *Appl. Phys. Lett.* **79**(10), 1546 (2001).
- <sup>25</sup>C. C. Chen, C. C. Yeh, C. H. Chen, M. Y. Yu, H. L. Liu, J. J. Wu, K. H. Chen, L. C. Chen, J. Y. Peng, and Y. F. Chen, *J. Am. Chem. Soc.* **123**, 2791 (2001).
- <sup>26</sup>J. D. Holmes, K. P. Johnston, R. C. Doty, and B. A. Korgel, *Science* **287**, 1471 (2000).
- <sup>27</sup>T. J. Trentler, K. M. Hickman, S. C. Goel, A. M. Viano, P. C. Gibbons, and W. E. Buhro, *Science* **270**, 1791 (1995).
- <sup>28</sup>T. J. Trentler, S. C. Goel, K. M. Hickman, A. M. Viano, W. Y. Chiang, A. M. Beatty, P. C. Gibbons, and W. E. Buhro, *J. Am. Chem. Soc.* **119**, 2172 (1997).
- <sup>29</sup>Y. Li, Y. Ding, and Z. Wang, *Adv. Mater. (Weinheim, Ger.)* **11**, 847 (1999).
- <sup>30</sup>A. M. Morales and C. M. Lieber, *Science* **279**, 208 (1998).
- <sup>31</sup>Y. Zhang, K. Suenaga, C. Colliex, and S. Iijima, *Science* **281**, 973 (1998).
- <sup>32</sup>D. P. Yu, C. S. Lee, I. Bello, X. S. Sun, Y. H. Tang, G. W. Zhou, Z. G. Bai, Z. Zhang, and S. Q. Feng, *Solid State Commun.* **105**, 403 (1998).
- <sup>33</sup>X. Duan and C. M. Lieber, *Adv. Mater. (Weinheim, Ger.)* **12**(4), 298 (2000).
- <sup>34</sup>J. C. Hulthén and C. R. Martin, *J. Mater. Chem.* **7**(7), 1075 (1997).
- <sup>35</sup>W. Han, S. Fan, Q. Li, and Y. Hu, *Science* **277**, 1287 (1997).
- <sup>36</sup>T. M. Whitney, J. S. Jiang, P. C. Searson, and C. L. Chien, *Science* **261**, 1316 (1993).
- <sup>37</sup>C.-G. Wu and T. Bein, *Science* **266**, 1013 (1994).
- <sup>38</sup>P. Yang and C. M. Lieber, *J. Mater. Res.* **12**(11), 2981 (1997).
- <sup>39</sup>P. Yang and C. M. Lieber, *Science* **273**, 1836 (1996).
- <sup>40</sup>Y. Q. Zhu, W. B. Hu, W. K. Hsu, M. Terrones, N. Grobert, T. Karali, H. Terrones, J. P. Hare, P. D. Townsend, H. W. Kroto, and D. R. M. Walton, *Adv. Mater. (Weinheim, Ger.)* **11**(10), 844 (1999).
- <sup>41</sup>J. L. Gole, J. D. Stout, W. L. Rauch, and Z. L. Wang, *Appl. Phys. Lett.* **76**(17), 2346 (2000).
- <sup>42</sup>F. Okuyama, T. Shibata, and N. Yasuda, *Appl. Phys. Lett.* **35**(1), 6 (1979).
- <sup>43</sup>F. Okuyama, *J. Cryst. Growth* **49**, 531 (1980).
- <sup>44</sup>F. Okuyama, *Appl. Phys. Lett.* **36**(1), 46 (1980).
- <sup>45</sup>G. N. Fursey, *IEEE Trans. Electr. Insul.* **20**(4), 659 (1985).
- <sup>46</sup>E. A. Litvinov, *IEEE Trans. Electr. Insul.* **20**(4), 683 (1985).
- <sup>47</sup>G. A. Mesyats, *Phys. Usp.* **38**(6), 567 (1995).
- <sup>48</sup>G. N. Fursey, L. A. Shirochin, and L. M. Baskin, *J. Vac. Sci. Technol. B* **15**(2), 410 (1997).
- <sup>49</sup>D. Li, Y. Wu, P. Kim, S. Li, P. Yang, and A. Majumdar, *Appl. Phys. Lett.* **83**(14), 2934 (2003).